Article:
Leco, M. orcid.org/0000-0002-4515-5327, McLeay, T. and Kadirkamanathan, V. orcid.org/0000-0002-4243-2501 (2022) A two-step machining and active learning approach for right-first-time robotic countersinking through in-process error compensation and prediction of depth of cuts. Robotics and Computer-Integrated Manufacturing, 77. 102345. ISSN 0736-5845

https://doi.org/10.1016/j.rcim.2022.102345

Robotics and Computer–Integrated Manufacturing 77 (2022) 102345

Contents lists available at ScienceDirect

Robotics and Computer-Integrated Manufacturing

journal homepage: www.elsevier.com/locate/rcim

A two-step machining and active learning approach for right-first-time robotic countersinking through in-process error compensation and prediction of depth of cuts

Mateo Leco [a,b,1,*], Thomas McLeay [a,c], Visakan Kadirkamanathan [b]

[a] Advanced Manufacturing Research Centre (AMRC), The University of Sheffield, Sheffield, UK
[b] Department of Automatic Control and Systems Engineering, The University of Sheffield, Sheffield, UK
[c] Sandvik Coromant AB, Stockholm, Sweden

ARTICLE INFO

Keywords:
Two-step process
Right-first-time machining
Robotic machining
Gaussian Process Regression
Data-driven models
Active learning

ABSTRACT

Robotic machining processes are characterised by errors arising from the limitations of the industrial robots. These robot-related errors can compromise the overall manufacturing process performance, resulting in final products with dimensions different from the nominal specifications. To avoid accumulation of errors through several manufacturing stages, a quality inspection step is usually performed after the cutting operation. This work presents an innovative two-step manufacturing method for achieving right-first-time characteristics in robotic machining operations through in-process inspection and compensation of the systematic errors, whilst collecting suitable training data for building predictive models. The key idea behind the proposed method is based on the observation that under certain conditions, the robotic machining errors remain largely consistent, and therefore by splitting the process into two similar steps and having an inspection step in between, a prediction and then compensation of the systematic errors would be possible. A Gaussian Process Regression (GPR) framework is applied for the creation of robust process models that predict the post-process inspection result from in-process signal features, with the associated confidence intervals. An active learning algorithm that makes online decisions on the inspection task based on the current confidence of the models, is also proposed. The two-step machining method and the active learning approach were both tested on a robotic countersinking process experiment. The results showed that the in-process inspection and error compensation of the proposed two-step machining method was able to achieve final countersink depths very close to the desired target, confirming the potential for right-first-time robotic machining. In addition, the active learning results highlighted the ability of the algorithm to reduce the number of required post-process inspections, thus saving both time and costs, whilst also identifying novel data relevant for the model training.

1. Introduction

Production systems in the aerospace industry are severely affected by scrap, especially in the case of high-value manufacturing processes. Therefore, in order to cope with the increase in product demand and remain competitive in the market, it is critical for such systems to deliver products of high quality right-first-time [1,2]. The recent developments in information technology and sensors capability, as well as the vision of Industry 4.0, have motivated manufacturers to increasingly push towards flexible and intelligent manufacturing systems. Such systems rely upon the use of auxiliary sensory information and data analytics tools for process monitoring and control [3,4]. In particular, a digital representation of the manufacturing process, also known as the 'digital twin', is applied to make autonomous decisions driven by machine learning algorithms based on the available process data [5]. In terms of the flexibility, robotic systems are becoming more and more popular in the manufacturing sector as an alternative of the traditional machine tools approach [6]. The aerospace industry could greatly benefit from the large working areas, multi-functionality and cost efficiency of industrial robots to help reduce production costs and increase the overall

* Corresponding author.
E-mail addresses: m.leco@sheffield.ac.uk (M. Leco), tom.mcleay@sandvik.com (T. McLeay), visakan@sheffield.ac.uk (V. Kadirkamanathan).
[1] Present address: Department of Automatic Control and Systems Engineering, The University of Sheffield, Amy Johnson Building, Portobello Street, Sheffield, S1 3JD, UK

https://doi.org/10.1016/j.rcim.2022.102345
Received 27 May 2021; Received in revised form 14 February 2022; Accepted 3 March 2022
Available online 11 March 2022

productivity. However, the variable stiffness and low positional accuracy of typical multi-joints industrial robots are the main factors that limit their adoption in machining operations, such as milling, drilling and countersinking. The quality of the end product is affected by the robot positioning within the workspace (i.e. the joints configurations), the required tool path and the forces applied during machining, resulting in deviations from the nominal specifications [7].

In addition to the above robot-related errors, the product material is another factor that influences the quality of the machined part. A popular choice in the aerospace industry is the Carbon Fibre Reinforced Polymer (CFRP). The advantageous properties of CFRPs, such as the light weight, high strength and stiffness, durability and excellent corrosion resistance, make this material ideal for the production of many large aircraft components. However, unlike with metals, the machinability of CFRPs with industrial robots is much more complicated due to their non-homogenous, anisotropic and very abrasive nature [8]. Typical machining problems include the delamination and pull out of fibres, rapid tool wear, as well as various surface anomalies. Research in this field [8,9] suggests that the choice of appropriate machining parameters (spindle speeds and feed rates) plays a key role in obtaining good quality parts. The optimal parameters are usually selected from experience or through several trials. Slamani et al. [10,11] studied the trajectory deviations occurred in high speed robotic trimming of CFPR parts and concluded that the robot positioning had also a major impact in the part quality in addition to the selection of the process parameters.

In general, the machining errors can be classified into two categories: systematic and random. The term systematic refers to errors that are repeatable and reproducible under similar conditions, whereas random errors vary. Chen et al. [12] subdivides the systematic errors further into constant-value and variable-value errors. The former are the errors caused by cutting tool miscalibration or workpiece misalignment and the latter include deformations induced by the machining forces and the tool wear. Random errors, on the other hand, are caused by different factors such as the non-homogeneous material properties, part deformations resulting from chatter and internal stress, etc., and they are difficult to compensate due to their non-reproducible nature.

To minimise the robot-related machining errors, several research studies in the robotic machining field have been investigating ways of improving the overall stiffness of the robot for the specific machining task. According to Ferreras-Higuero et al. [13], the robot pose is responsible for the vast majority (about 80%) of cutting tool deviations in robotic drilling operations. The main research themes include stiffness-based pose optimisation methods [14,15] and error compensation approaches [16–20]. Typically, accurate measurements of tool deflections that occur under the application of known external forces are required for the mapping of errors within the robot workspace. This information is then used to determine the optimal robot pose for the specific machining operation. Error compensation methods rely on force data and a compliance model of the robot for the estimation of force-induced tool deflections. These deflections can be simulated offline by the use of specific process models [16,17] or estimated online from the actual force measurements in closed-loop control schemes [18–20]. To improve system robustness and process accuracy, Zaeh et al. [21] proposed a combined approach, where the offline simulation of process forces and tool deflections was coupled with an online compensation mechanism based on spindle torque and vibration measurements for robotic milling applications. Focusing on the computational efficiency, Ge et al. [22] proposed a rapid prediction and compensation method based on reduction of global stiffness matrix for prediction of cutting force-induced errors in machining of thin-walled parts.

Machine Learning (ML)-based error compensation approaches [23–25] have also been proposed. Zhu et al. [23] applied artificial neural networks for mapping and compensation of robot positioning errors in robotic drilling of aircraft panels. A reduced two-dimensional workspace of the robot was considered to improve the efficiency of the compensation method. Wang et al. [24] proposed a statistical learning control method based on Gaussian Process Regression (GPR) [26] for trajectory tracking in laser cutting applications, where GPR models were used for both inverse robot dynamics and kinematics to compensate the torque and motor reference, respectively. The GPR framework has also been explored by Nguyen et al. [25] to model the dynamic properties of a typical six Degrees-of-Freedom (DoF) industrial robot used for milling operations. Other recent works that have reported the use of data-driven approaches for error prediction and compensation, focus on thermally-induced errors of conventional machining processes [27,28].

A common problem with ML-based approaches is their requirement for high volumes of training data. In high-value and low-volume manufacturing processes, the allocation of production time and workpiece material for the purpose of model training, is not sustainable. Consequently, strategies must be in place to allow for the collection of necessary training data during normal process operation whenever possible, or by introducing minimal disruption to the production line. Suitable data for the creation of ML-based predictive models can be provided by a post-process inspection step, however it would add extra costs associated with the time spend to perform this non-value-added operation, i.e. the inspection task. In this context, Papananias et al. [29] presented a method referred to as ‘inspection by exception’, which aimed to reduce the volume of post-process inspections in multistage manufacturing processes. A ML-based approach was applied on multistage data combined with in-process sensory information for the prediction of the quality of the end products, categorising them as conforming and non-conforming parts. Then, the inspection task was only needed in the cases when the predicted part quality could not be categorised in any of these categories with a high degree of certainty. Leco et al. [30] investigated the application of GPR models as part quality predictors in robotic countersinking operations. They used a data-driven approach to build and train a GPR model that predicts the post-process inspection result from the sensory information acquired during machining, with the potential to substitute the inspection step. However, to achieve accurate predictions, a dedicated experiment for the training phase of the model was required.

To overcome the high cost of obtaining labelled data for training of data-driven models, active learning approaches [31,32] have been adopted, where only a reduced subset of unlabelled samples (i.e. input instances) is considered for labelling. This subset is appropriately selected by the learning algorithm from a relatively large pool of unlabelled data. Active learning methods aim to achieve maximum prediction accuracy through identification of the most informative instances for training of the models, as opposed to a simple random selection of the same number of instances. Active learning can be performed offline when the entire pool of unlabelled data is available, or online [33] when the unlabelled data becomes gradually available (i.e. via data streams) and the decision for obtaining a new label is made online. This latter scenario is more appropriate for machining applications, where output labels provided by the inspection operation can be requested when needed and without process interruption, thus allowing the model to adapt to new process conditions. An application of active learning in manufacturing processes has been reported in Martinez-Arellano et al. [34], where Bayesian Convolutional Neural Networks (BCNN) were used for online tool condition classification. The model uncertainty representation of the Bayesian deep learning framework, coupled with an acquisition function was applied as a selection criterion to determine whether the incoming data required labelling, hence reducing the cost of model re-training. Botcha et al. [35] applied an active learning approach to reduce experimental cost in manufacturing processes. By using a sequential experimental design and choosing the next best experimental point based on a metric that reduces the expected uncertainty of the prediction, the active learning method reported a 65% reduction of the number of experiments for the same level of prediction accuracy, when compared with a model using random experimental points.

This paper extends the previous work of Leco et al. [30] by

introducing a two-step process method that allows compensation of the systematic errors arising from the robotic structure to obtain the desired part quality. It also allows a process model to be trained online without any process disruption, where the prediction accuracy is gradually increased as more data becomes available. This is done by adapting the 'inspection by exception' method of Papananias et al. [29] to robotic machining and incorporating an active learning approach. The relevance of each new instance with respect to the model training is assessed online as the input data is acquired and a decision on the inspection step is made, resulting in a reduction of the total number of inspections needed, without the performance of the model being compromised.

The two-step process method presented in this work aims to improve the performance of a robotic machining process by compensation of the robot-related systematic errors occurred during Step 1, in the attempt to obtain the desired part quality by the end of Step 2. An inspection measurement in between of the two process steps to collect the output labels is required for training of a data-driven predictive model using a supervised learning approach. A GPR framework combined with a perturbation-based data generation approach is applied to create robust models that predict the post-process inspection result with the associated confidence bands, based exclusively on in-process sensory information. In addition, to reduce the number of inspections, a two-step active learning algorithm that makes online decisions on the inspection task based on the current models' confidence, is proposed. It is shown that this method achieves the same degree of accuracy to the previous approach [30], but with a 52.6% reduction on average in the number of inspections.

To summarise, the main contributions of this paper are as follows:

1 The presentation of an innovative two-step process method that not only allows right-first-time manufacturing by inspection and compensation of the systematic machining errors, but also provides high quality training data for the creation of robust predictive models, without any process disruption.
2 The integration of an active learning approach for training of the models that minimises the total inspection costs, by actively deciding when a post-process inspection is required to further improve the prediction accuracy of the models.

The remainder of the paper is organised as follows: Section 2 presents the two-step manufacturing approach proposed by this work. Section 3 details the learning methodology applied to a robotic countersinking example and presents the two-step active learning algorithm. Section 4 describes the countersinking experiments conducted in a multi-robot platform. The results on decision making and the assessment of the proposed method's performance are discussed in Section 5. Finally, Section 6 outlines the conclusions of the paper. The GPR framework applied for the creation of the process models is presented in the Appendix.

2. A two-step approach for right-first-time robotic machining

The key idea behind the two-step process method is based on the observation that a cutting operation performed by an industrial robot is subject to comparable machining errors if the robot configuration is kept largely consistent during cutting. The method therefore splits the overall process into two similar steps and adds an inspection step in between to allow the prediction and then compensation of systematic machining errors arising from the robotic structure.

The diagram of the proposed two-step process method is illustrated in Fig. 1. The cutting operation of one process cycle is divided into two steps: Step 1 performs a first cut to a nominal target input specified by Target 1 (i.e. a semi-finished level) and Step 2 executes a second cut to the original nominal target input specified by Target 2 (i.e. the final level of finishing). At the end of Step 1, the machined part is inspected by an online inspection system to measure the output variable (Out 1) and then, prior to commencing Step 2, the input target is adjusted to reflect the systematic errors observed at Out 1. Note that the actual input targets (denoted by In 1 and In 2, respectively) also include a perturbation term that is required for training of the process models as explained in Leco et al. [30]. The final process output variable (Out 2) is obtained through inspection of the part at the end of Step 2.

Prediction of any systematic errors using in-process data requires the development of a data-driven predictive model with sufficient accuracy, which in turn demands the availability of rich training data that captures the varying cutting conditions. To this end, a perturbation signal is added to Target 1 and Target 2, producing cuts with different levels of finishing. It is important to note that this perturbation signal is programmatically controlled, and the same perturbation value is used for both steps that complete one full iteration of the process. This is to ensure that the input target of Step 2 would still aim towards reaching the desired level of finishing, regardless of the perturbation signal, thereby preserving the validity of the process iteration. Moreover, for greater data variability in model training, a new value of the perturbation signal is applied in every iteration of the process. This perturbation signal acts as an amplifier of any systematic errors occurring in the machining operation by simulating extreme input conditions.

Fig. 1 represents the two process models associated with each of the two steps of the same physical machining process. Architecturally, Model 1 and Model 2 are identical, with the inputs derived from processed sensor signals and the output being the prediction for the inspection result. However, the model mapping between Model 1 and Model 2 is different, since the actual input signals would have distinct signatures as result of the varying initial conditions of the workpiece between Step 1 and Step 2, noting that in Step 2 the part had already been machined to a semi-finished level.

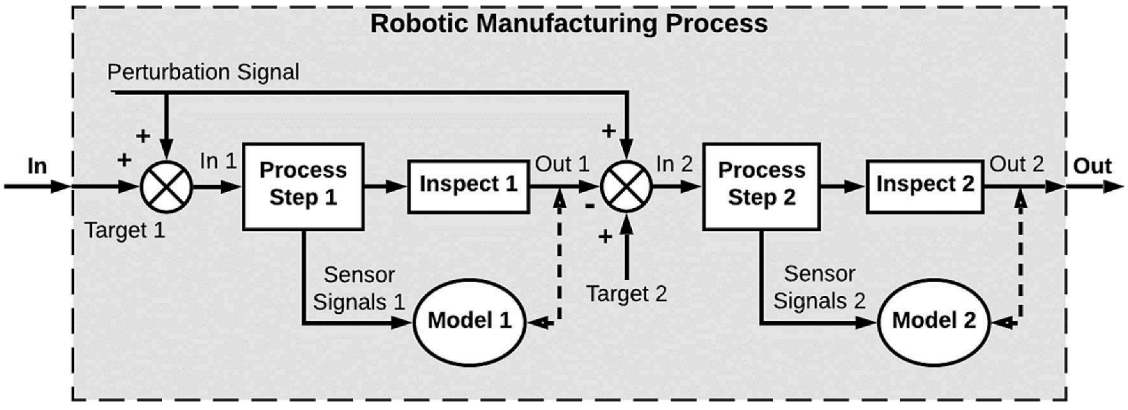

Fig. 1. Diagram of the proposed two-step process method.

With the introduction of the additional perturbation signal as shown in Fig. 1, the actual input target specified at the beginning of Step 1 is the sum of the nominal Target 1 and the perturbation value for that process iteration. Following Step 1, the measurement made at the inspection stage would be characterised with deviations from the actual input target by the machining errors. These errors include both systematic and random errors. In order to define the appropriate input target for Step 2, an output variable (Out 1 in Fig. 1) is derived by subtracting the nominal Target 1 from the inspection measurement. This output essentially captures a combination of the perturbation signal and the machining errors occurred in Step 1.

The actual input target for Step 2 is now not the nominal Target 2, but one that includes a correction that accounts for the systematic machining errors. This correction is derived by subtracting the output of Step 1 from the perturbation value. Proceeding with Step 2 and following the same logic as Step 1, the inspection measurement obtained after Step 2 would include the actual input target and the machining errors, both random and systematic that occurred in Step 2. A final output variable (Out 2 in Fig. 1) is derived as the difference between the above inspection measurement and the nominal Target 2. Due to the target correction at Step 2 that accounts for machining errors, this final output variable is now independent from the specific perturbation value, and it consists of the difference between the machining errors of Step 2 and those of Step 1 only. Consequently, by designing these two process steps as similar as possible in terms of the robotic configuration changes, cutting forces and material removal rate, the robot-related systematic errors would be eliminated. This will lead to Out 2 being close to zero and thereby achieving a level of finishing close to the desired final target, i.e. Target 2.

It is important to note that the proposed solution does not require any process interruption for collection of the training data necessary to build the two models. The programmatically controlled perturbation signal can be used to provide a suitable sample of input data (i.e. examples of sensor signals for different target levels) for training of Model 1. Then, the target correction process would ensure that this input data variability is carried over to Step 2 for training of Model 2. Note that the process Step 2 will still aim to reach the final desired level of finishing as result of the target correction. Both models can then be trained on the data collected from the normal operation of the process, without the need for a specific design of experiments. When sufficient training data have been acquired, the models would be able to provide predictions in substitution of the actual inspection measurement.

In terms of the modelling approach, this work considers a probabilistic framework based on Gaussian Process Regression (GPR) [26]. GPR models are naturally suited to deal with uncertainty in the input and output data and they can also provide useful extra information on the expected predictions, such as the intervals of confidence. Following previous work [30], a Square Exponential (SE) kernel performing Automatic Relevance Determination (ARD) was applied to reduce the input space of the GPR models. Further details on the GPR framework are presented in the Appendix of the paper.

3. Learning method for two-step robotic countersinking

This section presents the learning strategy of the proposed two-step process method applied to a robotic countersinking example.

3.1. Robotic countersinking example

A robotic machining example to test the two-step method is illustrated in Fig. 2. It consists of a countersinking process performed by two industrial robots working together in a master-slave setup. The diagram of Fig. 2a depicts the end-effector of the master holding the spindle and a pressure foot on the left side, a panel with a pre-drilled hole in the middle and the end-effector of the slave robot on the right side. These refer to the start and final positions of the robots, where both the master and the slave are assumed to be perfectly aligned to the hole centre and normal to the panel's surface. The countersinking process is illustrated in Fig. 2b, where the master, assisted by the pressure foot and in collaboration with the slave, clamps the panel while the cutting tool advances inside the pre-drilled hole to reach the desired countersink depth level. It is assumed that the spindle is operated by an external feed drive that controls the linear displacement of the cutting tool towards the surface of the panel independently, allowing therefore both robots maintain their original positions during the cutting operation. The process output variable is the countersink depth achieved as a result of the maximum level of penetration of the cutting tool inside the pre-drilled hole. The performance of the process is assessed in terms of the linear deflections of the countersinks, i.e. the deviation of the obtained countersink depths from the nominal target specified to the spindle controller.

Following the proposed two-step method, the process cycle of countersinking a single hole at the desired final depth can be divided into two similar steps: Step 1 would countersink the hole to a semi-finish level and Step 2 would finish countersinking to the desired final depth, after compensating for the observed systematic errors. To avoid introduction of further errors in between the two steps, it is assumed that the inspection step can be performed as part of the overall process cycle with both robots maintaining their original positions. In this example, the pressure foot would need to be temporarily retrieved to allow a clear view of the machined hole at the end of Step 1 and prior to starting Step 2, however, the master robot needs not change its position to do this, as the pressure foot is operated independently.

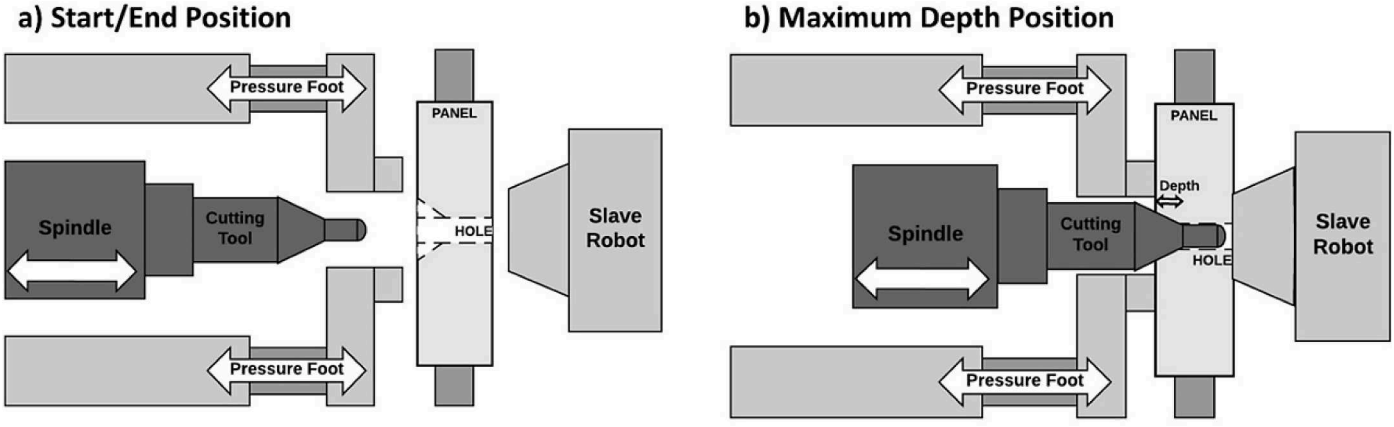

Fig. 2. Robotic countersinking diagram: a) start and final positions of master and slave robots; b) position of maximum depth obtained by the countersinking process.

3.2. Two-step active learning procedure

The diagram of the two-step active learning procedure and its legend are illustrated in Fig. 3 and Table 1, respectively.

The steps of the proposed learning approach for the countersinking of a single hole are as follows (ref. to Fig. 3):

1 The process commences by specifying a target depth (T_1) for the cutting operation. The first cut is performed to a pre-set semi-finished level (D_1) and an additional perturbation value (P), randomly selected from the zero mean Gaussian perturbation signal $P \sim \mathbb{N}(0, \sigma_p^2)$ with standard deviation σ_p.

2 In-process sensor signals (S_1) are acquired and a depth prediction with mean ($\widehat{Y}_1$) and standard deviation ($\widehat{\sigma}_1$) is provided by the GPR model (Model 1) at the end of the first cut. The model uses the current dataset for making predictions and it requires a minimum amount of training data, which needs to be specified in advance.

3 Based on $\widehat{\sigma}_1$, a decision on inspecting the machined hole for a direct depth measurement is made. For $\widehat{\sigma}_1$ greater than a pre-set uncertainty threshold (θ_1), the model confidence in the prediction is low due to the high uncertainty levels, indicating that $\widehat{Y}_1$ is likely to be not accurate and thus a direct measure (Y_1) is necessary. If, however, $\widehat{\sigma}_1$ shows low uncertainty levels, indicating a high confidence in $\widehat{Y}_1$, then there is no need to inspect the hole. For every inspection that is requested, the pair (S_1, Y_1) is included in the current training dataset (Dataset 1) of Model 1.

4 Depending on the inspection decision at step 3, a depth error value ($\widehat{E}_1$ or E_1) is calculated from $\widehat{Y}_1$, the estimated from Model 1, or Y_1 obtained from the inspection process.

5 This depth error is then used to correct the target depth of the second cut (T_2), accounting also for the perturbation value added in the first cut. This is achieved by subtracting the depth error and then adding the perturbation value to the desired final depth level (D_2).

6 Once T_2 has been specified, the second cut can start and the above steps 2, 3 and 4 are repeated for the second cut, referring to its own

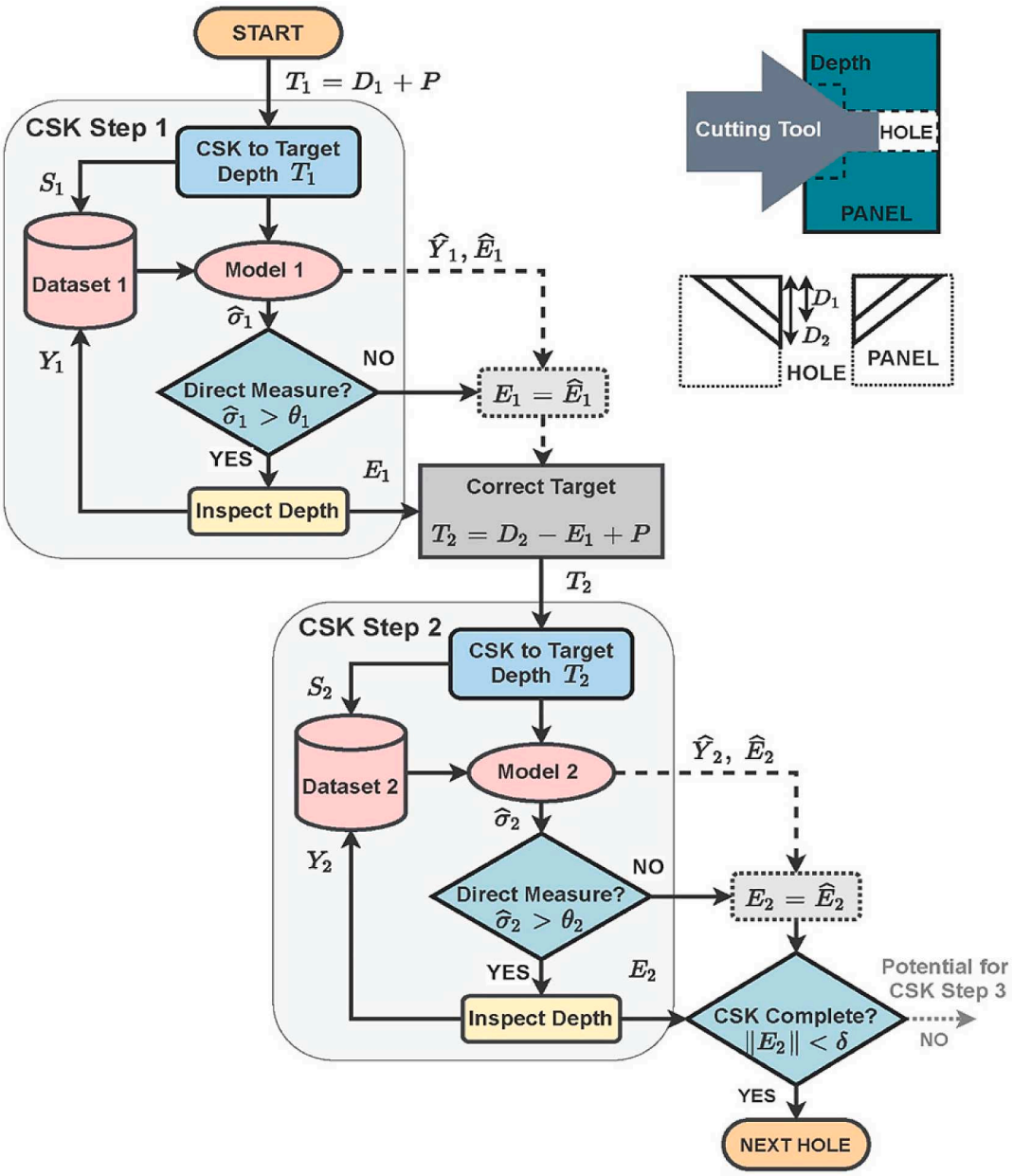

Fig. 3. Diagram of the proposed two-step active learning procedure.

Table 1
Legend of the two-step active learning diagram.

S_n	Sensor signals
D_n	Nominal depth (desired level)
P	Perturbation signal
T_n	Process target depth
Y_n	True depth measurement (from inspection)
$\widehat{Y}_n$	Estimated depth (GPR-predicted mean value)
$\widehat{\sigma}_n$	Estimated uncertainty (GPR-predicted standard deviation)
E_n	True depth error (calculated as $Y_n - D_n$)
$\widehat{E}_n$	Estimated depth error (calculated as $\widehat{Y}_n - D_n$)
θ_n	Uncertainty threshold
δ	Process depth tolerance

(*) n specifies the cutting number of a hole of the panel.

data, i.e. sensor signals S_2, direct measurement Y_2, Model 2 with predictions $\widehat{Y}_2$ and $\widehat{\sigma}_2$, uncertainty threshold θ_2 and depth error $\widehat{E}_2$ or E_2.

7 Finally, the amplitude of E_2 is checked against the process depth tolerance (δ). If successful, the process continues to the next hole, otherwise an option to perform a third cut can be offered by applying the latest depth error E_2 to correct the target depth. Note that this is only possible if the actual depth has not exceeded the process tolerance, i.e. for negative values of E_2 (shallow holes).

The active learning is achieved by allowing the algorithm to select which output label (i.e. inspection of the machined hole) would improve the current prediction accuracy of the model. This is done by setting an uncertainty threshold on the variance output of the GPR model. An inspection is then required when the variance output is higher than the above threshold, meaning that the model confidence estimation of the current prediction is relatively low. Note that the variance output of the GPR model is computed from the newly acquired input data (i.e. sensor signals) and the current dataset of the model. In this scenario, every time an inspection is requested by the algorithm, the corresponding output data is added to the current dataset and therefore it is made available for training of the model for all subsequent predictions.

The following gives an error analysis of the two-step active learning procedure shown in Fig. 3. The true countersink depth obtained after the first cut (Y_1^i) for the i^{th} hole can be expressed as (see also Table 1 for the terminology):

$$Y_1^i = T_1^i + N_1^i = D_1 + P^i + N_1^i \tag{1}$$

where N_1^i represents the overall noise that the machining process introduces during the first cut of the i^{th} hole and $P^i \sim \mathbb{N}(0, \sigma_p^2)$ is the programmatically added, normally distributed, perturbation value of the i^{th} hole. The desired (nominal) depth of the first cut D_1 is kept unchanged for all the holes. Consequently, the true depth error of the first cut (E_1^i) is given by:

$$E_1^i = Y_1^i - D_1 = P^i + N_1^i \tag{2}$$

The target depth of the second cut (T_2^i) for the i^{th} hole, chosen to compensate the first cut depth error, and accounting for the perturbation signal, is given by:

$$T_2^i = D_2 - E_1^i + P^i \tag{3}$$

where D_2 is the desired final depth, kept the same across all the holes. Similarly, the true depth value of the second cut (Y_2^i) will be influenced by the process noise (N_2^i). To identify the correct sources of errors in the process, further consideration is required in this case. After performing the first cut, the master robot needs to unclamp the panel to allow a clear view of the machined hole for the inspection process to take place. This involves retracting the pressure foot, acquiring an image of the machined hole and then activating the pressure foot again to clamp the panel for the start of the second cut. To minimise other potential error sources, it is assumed that both robots maintain their original positions during this re-clamping process and for the entire duration of the second cut. Consequently, the true depth of the second cut can be expressed as:

$$Y_2^i = T_2^i + N_2^i + N_r^i \tag{4}$$

where the additional term N_r^i refers to the noise caused by the re-clamping process for the i^{th} hole and N_2^i is the overall noise introduced by the machining process during the second cut, similar to the case of the first cut. The substitution of Eq. (2) and Eq. (3) into Eq. (4) leads to the expression below for Y_2^i:

$$Y_2^i = D_2 + N_r^i + \left(N_2^i - N_1^i\right) \tag{5}$$

Considering that the position and orientation of the robots remain unchanged while cutting and inspecting the same hole, and that the high clamping forces would minimise any panel movement during machining, it is safe to assume that the re-clamping noise N_r^i would be of a negligible amount. Moreover, the application of the pressure foot helps to reduce the errors caused by the different cutting forces between the first and the second cuts due to the target differences. The magnitude of the clamping forces can be set sufficiently higher to ignore those small variations in the process loads between the two cuts. Consequently, the current hole position (i.e. the configuration of the robots) and the clamping forces represent the main sources of systematic errors into the overall countersinking process. This means that when machining the same hole, the systematic errors will be expected to be the same for both cuts, whereas when the process goes from one hole to the next, a different error will be introduced as result of the changes in the robot positioning. Hence, the two process noise terms of Eq. (5) can be described as:

$$N_1^i = B^i + Q_1^i, \; N_2^i = B^i + Q_2^i \tag{6}$$

where Q_1^i and Q_2^i are the random errors with zero mean and B^i is the common systematic error of the i^{th} hole. Substitution of the noise terms of Eq. (6) in Eq. (5) gives:

$$Y_2^i = D_2 + N_r^i + \left(Q_2^i - Q_1^i\right) \tag{7}$$

which leads to the final true depth error (E_2^i) defined as:

$$E_2^i = Y_2^i - D_2 = N_r^i + \left(Q_2^i - Q_1^i\right) \tag{8}$$

This shows that the final depth error has a negligible term due to re-clamping and two random process errors with all systematic errors being removed. Statistically, the expected value of the error would be zero.

In the case of using the model depth predictions instead of the true camera measurements, another error term related to the model prediction error needs to be considered in the above computations. By definition, the model error (M) is derived as the difference between the true depth measurement (Y) and the predicted depth ($\widehat{Y}$), i.e. $M = Y - \widehat{Y}$. When these model errors are included in the above analysis, the estimated depths at the end of the first cut ($\widehat{Y}_1^i$) and the second cut ($\widehat{Y}_2^i$) of the i^{th} hole can be expressed as:

$$\widehat{Y}_1^i = D_1 + P^i + N_1^i - M_1^i \tag{9}$$

$$\widehat{Y}_2^i = D_2 + N_r^i + \left(Q_2^i - Q_1^i\right) - \left(M_2^i - M_1^i\right) \tag{10}$$

where M_1^i and M_2^i are the model prediction errors for the i^{th} hole of Model 1 and Model 2, respectively. Hence, the estimated depth error ($\widehat{E}_2^i$) of the i^{th} hole is as follows:

$$\widehat{E}_2^i = \widehat{Y}_2^i - D_2 = N_r^i + \left(Q_2^i - Q_1^i\right) - \left(M_2^i - M_1^i\right) \tag{11}$$

This error is also likely to be small since the systematic model

prediction errors from the two different steps of the process are removed. Moreover, the performance of the GPR models improves with the increasing size of training data, therefore the prediction errors would tend towards zero through continual growth of the dataset.

3.3. Learning algorithm

This section presents the implementation of the proposed learning approach in an algorithmic form. The pseudocode of the two-step active learning algorithm is described in Table 2.

The first two lines of the algorithm set the learning parameters as well as initialise the current dataset (DS) and feature subset (FS) variables of both models. Line 3 marks the start of the process iteration for the current hole. The lines 4-8 ensure that the current training dataset grows to the appropriate size required for the GPR model to start making predictions. Note that this is done only at the beginning of a new process, where no training data is available. In this stage, the inspection step is requested after every cut and the size of the dataset increases as more cuts are performed. The GPR model will be trained once the pre-defined initial DS size has been reached. Each model refers to its own dataset, as indicated in Fig. 3.

In line 10, a new input data corresponding to the features extracted from the sensor signals is acquired. Line 11 monitors changes in the size of the dataset during the previous iteration indicating that new data has been added. If that is true, then the model is re-trained accordingly (lines 12-13). The feature selection step based on the ARD-SE kernel (ref. to Eq. (12) in the Appendix) has also been applied as part of the GPR training process. The current FS is updated to include the newly selected features (line 12). A pre-set minimum FS size is necessary to prevent the algorithm from selecting too few features when little information is available, especially at the beginning of the procedure. Once the relevant features have been selected, the GPR model can use a Squared Exponential (SE) kernel for faster re-training and prediction on new data. An updated GPR-SE model is then re-trained using the current DS and FS (line 13).

A model prediction of the newly acquired input data is given in line 15, where the current GPR-SE model provides a mean value ($\widehat{Y}$) and standard deviation ($\widehat{\sigma}$) of the estimated countersink depth. A check on $\widehat{\sigma}$ follows in line 16: if $\widehat{\sigma}$ is greater than the uncertainty threshold (θ), corresponding to high levels of uncertainty in the prediction, then an inspection is required to measure the actual countersink depth, calculate the true depth error and then include it into the current DS (lines 17-18). Otherwise (for $\widehat{\sigma} \leq \theta$), an inspection is not needed due to the model showing high enough confidence. In this case, an estimated depth error computed from $\widehat{Y}$ can be used instead of the true depth error (line 20). Note that in the absence of new output data from the inspection step, there are no changes to the current GPR model, DS and FS.

Line 22 differentiates the cases based on the current cut number. If all the above steps were referring to the first cut, then the entire procedure (from line 10) is repeated for the second cut (i.e. the process Step 2), with reference to its own current GPR model (i.e. Model 2), DS and FS (line 23). Finally, once the second cut is performed, the process can proceed to the next hole (line 25). This completes a single iteration of machining a hole using the two-step active learning procedure.

Table 2
Pseudocode of the two-step active learning algorithm.

	Two-Step Active Learning Algorithm
1	**Set parameters:** initial Dataset (DS) size; min Feature Subset (FS) size; uncertainty threshold (θ)
2	**Initialise variables:** DS and FS of both models
3	Begin process iteration for the current hole
4	**if** DS size < initial DS size **then**
5	Acquire a new pair of input-output data (i.e. signal features (S) and depth measurement (Y))
6	Calculate the true depth error (E) and update DS
7	Repeat steps 5-6 above for the second cut (referring to its own DS)
8	Proceed to the next hole of the panel (repeat from step 3 above)
9	**end if**
10	Acquire new input data (i.e. the feature vector extracted from S)
11	**If** DS was previously updated **then**
12	Reduce input space (ARD method) and update FS
13	Re-train GPR-SE model with the updated FS and DS
14	**else**
15	Apply current GPR model to obtain a prediction mean ($\widehat{Y}$) and standard deviation ($\widehat{\sigma}$)
16	**if** $\widehat{\sigma} > \theta$ **then**
17	Request an inspection (get a new depth measurement Y)
18	Calculate the true depth error (E) and update DS
19	**else**
20	Compute the estimated depth error ($\widehat{E}$) from the model prediction ($\widehat{Y}$)
21	**end if**
22	**If** the depth error refers to the first cut **then**
23	Repeat steps 10-21 above for the second cut (referring to its own DS and FS)
24	**else**
25	Proceed to the next hole (repeat from step 3 above)
26	**end if**
27	**end if**

4. Robotic countersinking experiments

This section describes all the experimental work conducted for the development and testing of the proposed two-step active learning approach.

4.1. Robotic platform and inspection system

The robotic platform considered in this work consisted of two industrial robots (KUKA): a large master robot (model KR360) with a countersinking end-effector and a (relatively) small slave robot (model KR180), as shown in Fig. 4. An external drive attached to the master's end-effector was applied to control the spindle movement along the feed direction for the countersinking task. The master was also equipped with an air-driven pressure foot to assist during machining, while the end-effector of the slave served as an anvil to counteract the process load. RoboTeam software was installed on both robot controllers (Kuka KRC2) to enable co-ordination of their movements and a central control system was used for the robots' end-effectors.

The machining application performed by the robots was the countersinking of pre-drilled holes in Carbon Fibre Reinforced Polymers (CFRP) panels of the aircrafts. The panel was located in between the two robots inside their shared workspace and was secured by means of two fixtures. The process operation included the following steps:

- Both master and slave robots moved in proximity of a pre-drilled hole (one robot on either side of the panel).
- A Lucana Aero vision system integrated with the robots' controller was used to guide the robots for precise localisation of the hole centre, while maintaining normality to the surface of the panel.
- Once in position, the slave advanced slowly towards the back side of the panel until contact was made and then stopped, waiting for the master.
- The master activated the pressure foot and, in conjunction with the slave, clamped the panel to a pre-set force. This event marked the beginning of the cutting cycle.
- Both robots remained in position holding the panel, while the spindle drive advanced the cutting tool towards the panel's surface for countersinking of the hole to a specified target depth.
- After reaching the specified countersink depth, the spindle returned to its home position and the master retracted the pressure foot to

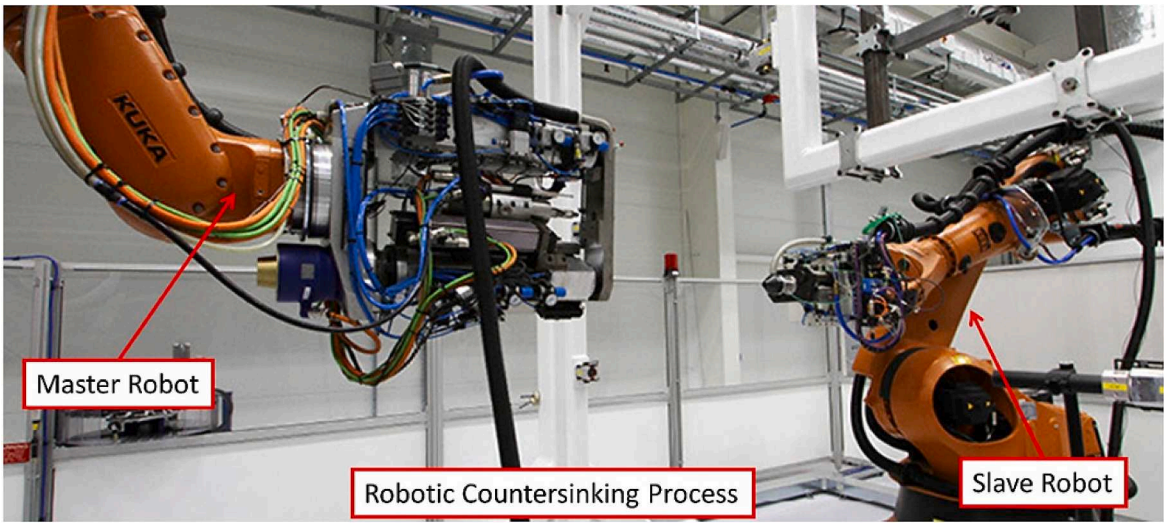

Fig. 4. Robotic platform used for the countersinking process: Master robot (left) and Slave robot (right).

unclamp the panel. Both master and slave returned simultaneously to the starting positions.
- The process proceeded to the next hole of the panel.

A notional tolerance of +/- 0.2 mm of the countersink depth deviations influenced the setup of the robotic cell. Note that the angular deflections were minimised due to the use of Lucana Aero system for precise hole alignment prior to the cutting process and the application of the pressure foot (i.e. the clamping forces) during machining. Consequently, the angular deflections of the countersinks were not considered in this work. To minimise the delamination problem related to the machinability of CFRP panels, preliminary trials using different tool geometries and machining parameters were conducted outside the scope of this work.

The inspection system consisted of a Cognex camera equipped with telecentric lenses, as illustrated in Fig. 5 (right). It was used to inspect the countersink depth after each cut of every single hole. An example of a CFRP panel with 44 countersunk holes obtained from the experiments is shown on the left side of Fig. 5. The inspection step was included in the process operational cycle to allow direct measurements of the output variable without any process interruptions. An image of the hole was acquired as soon as it was machined and then processed to compute the countersink depth. To align the camera with the hole, a pivoting mechanism attached to the master's end-effector was applied. It was able to switch between two pre-set positions as required: tool position for machining and camera position for the inspection task. Note that the use of telecentric lenses allowed capturing consistent images of the machined holes, independently of their distances from the camera.

To accommodate the inspection routine, the following steps were added to the overall machining process:

- After countersinking the hole, the spindle moved back to the home position and the pressure foot was retracted.
- The pivot drive switched to the camera position and moved the camera slightly forward for the image acquisition. This image was then sent to the PC for processing and extraction of the countersink depth.
- The camera returned to its home position and the pivot drive switched to the tool position.
- The process moved to the next hole.

The above extra inspection steps increased the overall process operational cycle by approximately 7-8 seconds, however the process output variable was measured in real time, as more holes were

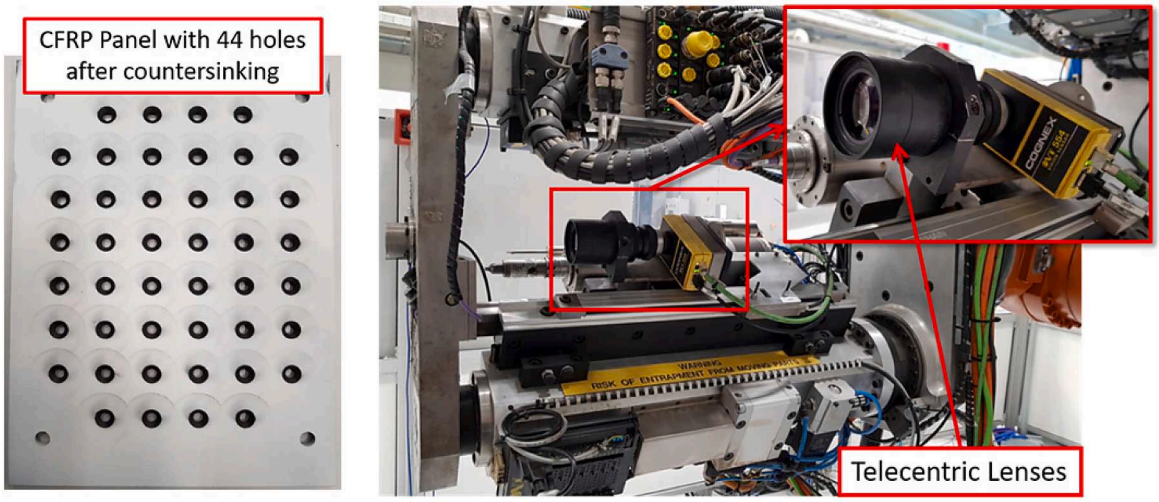

Fig. 5. Inspection system: CFRP panel after countersinking (left) and Congnex camera with telecentric lenses (right).

machined. The accuracy of the inspection method in the computation of the countersink depth errors (i.e. the linear deflections of the countersinks) from the images of the machined holes was in the range of +/- 0.05 mm.

4.2. Experimental setup and data acquisition

An experiment using the above robotic platform was conducted to test the proposed two-step process method. A total of 308 holes (seven panels of 44 holes each) were machined. Each CFRP panel had 44 predrilled holes regularly distributed in a rectangular grid of dimensions $30 \times 21 \times 7$ mm. The purpose of the experiment was to evaluate the two-step approach and obtain the data required for the creation and training of predictive models. In particular, the sensor signals collected during machining (input data) and the inspection measurements of the machined holes (output data) served as a training dataset to build Gaussian Process Regression (GPR) models for the prediction of the observed countersink depth deviations.

The experiment was conducted following the two-step method described in Section 2: two cuts were performed for every single hole of the panel with nominal depth targets $D_1 = 2mm$ (semi-finished level) and $D_2 = 2.74\ mm$ (final level). The actual depth target specified as input for the countersinking process was set in accordance with the two-step learning procedure shown in Fig. 3: the first cut was targeted at T_1 and the second cut at the adjusted target T_2. The perturbation signal was a zero-mean Gaussian distributed variable with standard deviation $\sigma = 0.25$. A new value of the perturbation signal was randomly selected for every hole of the panel. At the end of each cut, an image of the machined hole was captured by the inspection camera and the corresponding countersink depth (i.e. the process output variable) was computed. All the cuts were performed using the same cutting tool (a two-flute countersinking tool) and tool wear was assumed to be negligible. The machining parameters were set as: spindle speed 4978 RPM (Rotations per Minute); feed rate 298 mm/min; force target of the pressure foot 500 N.

The data acquisition hardware included two high frequency accelerometers (single axis) for vibration measurements, an Acoustic Emission (AE) sensor, a power transducer and a linear encoder. A central data acquisition device (NI cDAQ-9178) was used to connect all the sensors and ensure the synchronisation of multiple sensors signals with different sample rates. All the data was acquired and then processed to extract various signal features using NI LabVIEW software. One of the vibration sensors was mounted on the spindle holder to measure the tool vibration in the feed direction (master's Z axis) and the other was attached to the pressure foot body to measure the vibration in the perpendicular direction (master's X axis). The AE sensor was installed on the pressure foot near the cutting area. The power transducer was placed inside the robot controller box and provided spindle power data. The linear encoder acted as an acquisition trigger for the other sensor data. It was used to detect the pressure foot movement during the clamping process at the start of every cut, which was a repeatable event and therefore perfect for the automatic triggering task.

In order to convert the raw sensor data in useful features that can represent the cutting process, a number of signal processing techniques were applied. These involved various filtering methods (low-pass, band-pass and running RMS data), signal segmentation (automatic extraction of the cutting region) as well as analysis of the signals in time and frequency domains. The processing scheme was specific to the signal type and further details on the extracted signals can be found in Leco et al. [30].

In terms of the signals features, common statistical descriptors were extracted from the segmented signals. These included the signal mean, RMS, variance, skewness, kurtosis, peak (or peak-to-peak) and crest factor. Some additional features, such as the cutting cycle duration (time-in-cut) and the time to reach the signal peak (time-to-peak) were also considered. The frequency domain was assessed in terms of the Power Spectral Density (PSD) of the time data. Here, the above statistical features were extracted from two main spectra: the original PSD of the signals and the selected PSD bands. These bands were specific to the signal type and further details on the extracted features can be found in Leco et al. [30]. A total number of 230 features were extracted, including two that were independent of the signals, but carried information about the hole number and position within the 44-holes pattern of the panels.

4.3. Countersink depth measurements

The countersink depth measurements obtained upon inspection of the machined holes after the first cut (in blue) and after the second cut (in red) are illustrated in Fig. 6. The horizontal dashed lines indicate the two nominal depth targets (denoted by D_1 and D_2) and the vertical dotted lines refer to the panel indices.

Fig. 6 highlights the presence of a systematic error in the countersink depths obtained from the first cuts, which resulted in most of the holes being over the desired target $D_1 = 2\ mm$. Note that these cuts were originally set to a target with a zero mean random perturbation and centred at D_1. The systematic error observed in the countersink depths of the first cuts was associated to a tool calibration error and, as shown in the depths of the second cuts, this was compensated by the target correction of the two-step process method. The large data variability introduced by the perturbation signal in the first cuts was also

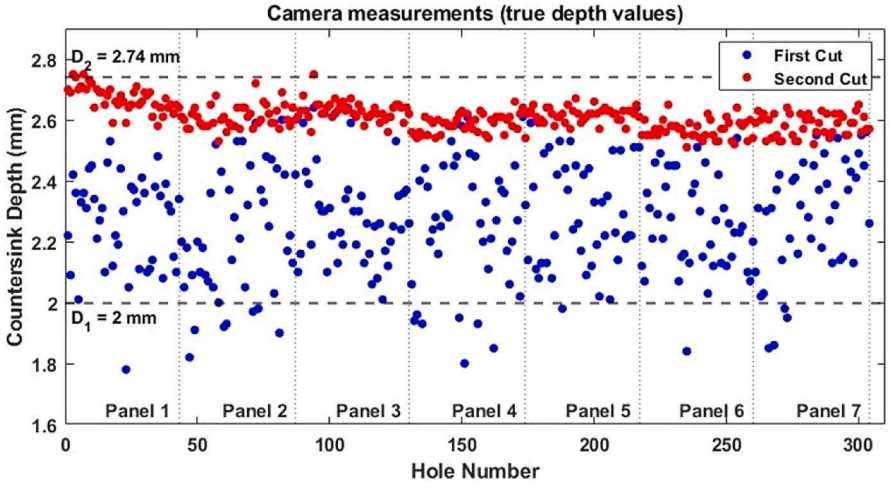

Fig. 6. Countersink depth measurements obtained from the experiment.

significantly reduced in the case of the second cuts, resulting in final depths within the +/- 0.2 mm tolerance from the nominal target $D_2 = 2.74$ *mm*. These depth measurements confirm the effectiveness of the two-step method to deliver right-first-time countersinking features in the considered case study.

5. Results and discussion

This section discusses the results obtained by the proposed learning approach for the robotic countersinking case study. Even though the procedure considered reducing the number of inspections, all holes were inspected in order to test the performance of the learning method. Only the data that was required for inspection as part of the learning procedure was used in model building and decision making, and the holes that didn't require inspection were only used in performance assessment. The two datasets of the learning problem consisted of the features extracted from the acquired sensor signals and the depth data provided by the inspection system, with respect to the first and second cut. Model 1 and Model 2 were trained using instances of the extracted signal features (i.e. the feature vectors) as input data and the corresponding countersink depth as output data, obtained from the first and second cuts, respectively.

5.1. Decision-making results

The two-step active learning procedure requires an initial dataset for the GPR models to start making predictions. In a production scenario, this can be obtained by performing the inspection task and collecting the camera measurements for a pre-set number of process iterations (i.e. the initial DS size). In the tests here, the initial dataset consisted of a fixed number of holes that were cut from Panel 1, up to the whole of Panel 1. Another parameter that requires specification in advance is the uncertainty threshold (θ), defined on the standard deviation ($\widehat{\sigma}$) output of the GPR model. This is also the key parameter that determines the decision on whether to inspect or not. Finally, the last parameter to set in advance corresponds to the minimum size of the Feature Subset (FS). The feature selection strategy consisted in the selection of a reduced subset of features according to the ARD-SE feature selection method described in the Appendix. Initial choices of these three parameters were inferred from prior knowledge of the process and cross-validation tests performed on the two datasets (one for each model) obtained from the experimental work. A minimum FS size of 20 and an uncertainty threshold of 0.06 mm were selected for both models. The initial DS size was set at 43 corresponding to the whole of Panel 1. Note that due to the bad signal quality, one of the holes of Panel 1 (hole number 42) was excluded from the dataset, leaving Panel 1 with a total of 43 holes.

The results of the two-step active learning algorithm in terms of decision-making on the inspection task are shown in Fig. 7a) Model 1 and b) Model 2. The predicted standard deviations $\widehat{\sigma}$ are illustrated by the blue vertical bars and the uncertainty threshold θ (applied to $\widehat{\sigma}$) is indicated by a horizontal red line. For reference, the panel indices are also shown in the figure by the vertical dashed lines.

One of the key features of the two-step active learning procedure is the reduced need for inspection if sufficient confidence in the model's predictions is achieved and, at the same time, the inclusion of the inspection measurements into the training dataset for all the cases of predictions with higher uncertainty. Note that most of the predicted standard deviations are below the uncertainty threshold for both the models, indicating that, in most cases, sufficient information was available at the time the models made the predictions. This means that the proposed decision-making method of requesting an inspection only for the cases where $\widehat{\sigma} > \theta$, has successfully reduced the total number of post-process inspections. This characteristic is better illustrated in Fig. 8,

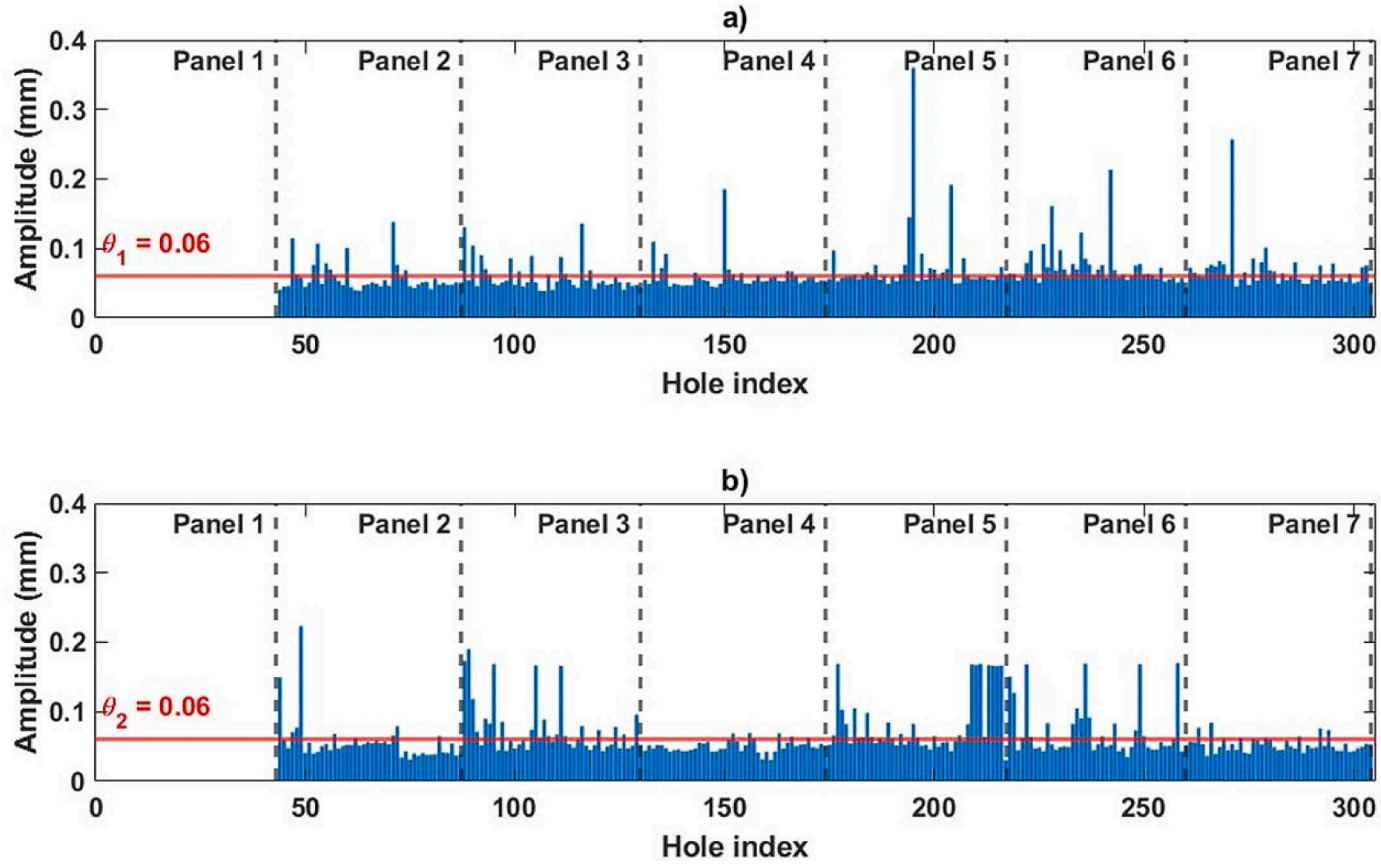

Fig. 7. Predicted standard deviations obtained from the GPR models according to the two-step active learning algorithm: a) Model 1; b) Model 2.

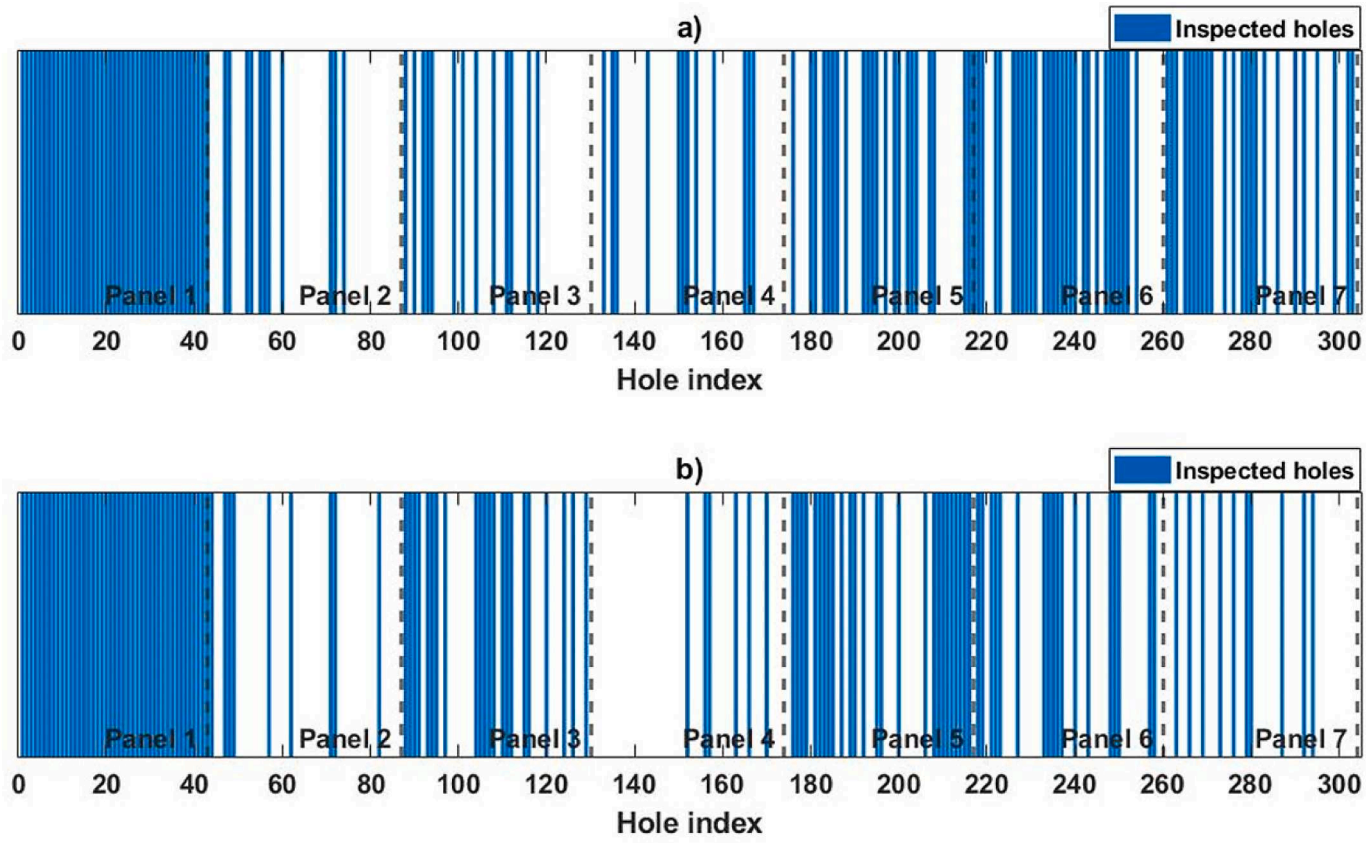

Fig. 8. Inspections requested by the two-step active learning algorithm: a) Model 1; b) Model 2.

where the indices of all inspected holes, as requested by the two models, have been highlighted: a) Model 1 and b) Model 2. Only the depth measurements of the inspected holes were included into the training dataset, and thus, made available for all subsequent model predictions. At the end of the procedure, the final DS size was 154 for Model 1 and 134 for Model 2, representing 50.7% and 44.1% respectively, of the total number of machined holes.

The results of Fig. 8 show that for both models, the learning algorithm had requested to inspect one or more holes from each of the panels considered in the experiment. In the case of Model 1, the initial dataset composed of Panel 1 provided sufficient information for the GPR model to confidently predict the countersink depths of most holes from panels 2, 3 and 4. Here, the intervention of the inspection camera was occasionally requested by the learning method. In contrast, the holes of Panel 5 were inspected more often, indicating that the acquired in-process signals were probably slightly different from those observed in the presiding panels. Panel 6 and the start of Panel 7 required frequent inspections too, until sufficient data were collected to make confident

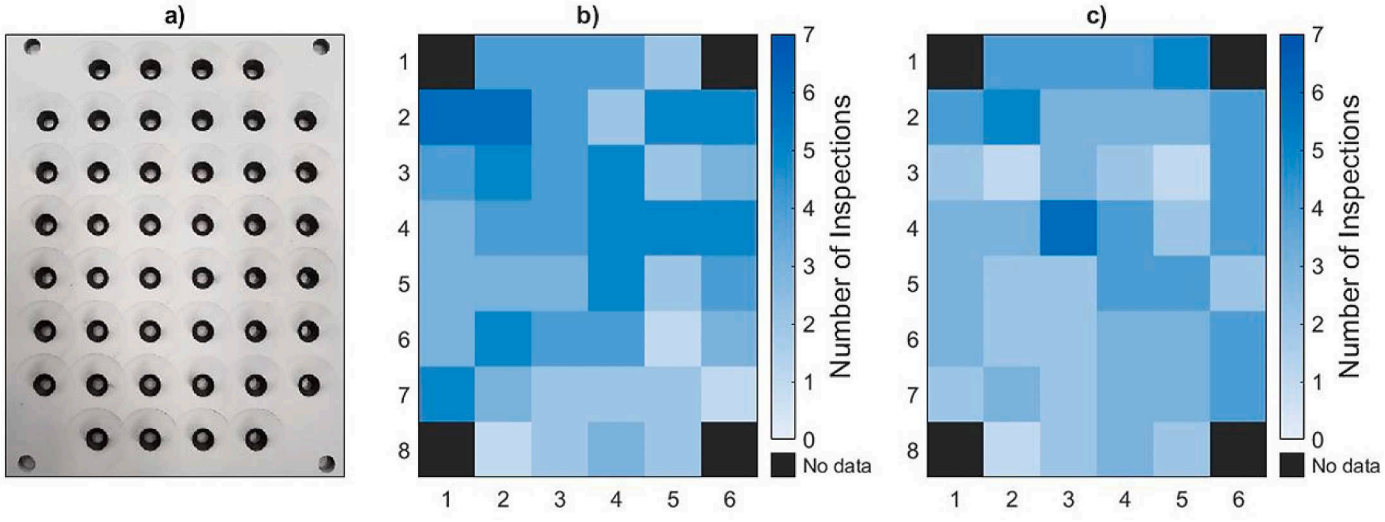

Fig. 9. A heatmap representation of the number of inspections per hole requested by the two-step active learning algorithm in accordance with the spatial layout of the panel: a) CFRP panel; b) Model 1; c) Model 2.

predictions for the depths of the remaining holes of Panel 7. Similarly, Model 2 was able to achieve a high level of confidence in the prediction of most depths of Panel 2 after training on the data from Panel 1 initially. Frequent camera interventions at the beginning and middle of Panel 3, further increased the confidence of model for the depth predictions of Panel 4. The start of Panel 5 required more inspections, suggestive of a small change in the process conditions. Frequent camera measurements were also requested at the end of the Panel 5 and through the start of Panel 6. Differently from Model 1, Panel 6 didn't require so many inspections for Model 2. There were only a few holes around the middle of the panel that were occasionally inspected. For Panel 7, direct measurements were occasionally needed during the first half of the panel, indicating that the model had built up sufficient training data to make depth predictions with a high level of certainty for the remaining holes.

Finally, Fig. 9 illustrates a heatmap representation of the inspected holes arranged following the panel layout for both models: a) CFRP panel; b) Model 1 and c) Model 2. This representation highlights the regions of the panel that required more inspections. Out of seven panels in total, the maximum times that the same hole position was inspected across the panels was six, whereas the minimum was one time. It can also be observed that consistent results between the two models were achieved from the learning algorithm.

The two heatmaps of Fig. 9 reveal that the top half of the panels was inspected more often than the bottom half for both models (165 vs. 123 in total), meaning that the knowledge acquired by the inspection of these first few holes of each panel had useful information for the models to improve their confidence in the prediction of the countersink depths of the remaining holes. The small variations in the number of inspections are due to the random perturbation signal added to the target depth, giving rise to slightly different (un-modelled) process conditions as reflected through the in-process signals.

5.2. Performance assessment

Although the goal of the two-step active learning algorithm was to reduce the total number of the post-process inspections, all the holes machined during the experiment were inspected after each cut and their countersink depth data was used for assessing the performance of the proposed approach.

It is important to note that the two outputs of the GPR model, the depth prediction and its standard deviation, were computed based on the currently available dataset of the model at the time that the prediction was made. For instance, when attempting to predict the countersink depth of a hole in Panel 2, the model would rely on the information collected from the whole of Panel 1 and any other data from Panel 2 that have previously been included into the training dataset. Consequently, in the experiment considered here, the largest dataset would be available for the holes of the last panel (Panel 7). Also, in a real-time scenario, if the algorithm decides to skip the inspection step and use the model prediction instead, then the actual depth measurement won't be available to compute the prediction error. In the following, however, for evaluation purposes, the prediction errors are reported for all the cuts performed in the experiment, regardless of the algorithm's decision on the inspection step.

A scatter plot of the depth prediction error against the GPR predicted standard deviation for each hole is given in Fig. 10 for both models: a) Model 1 and b) Model 2. The uncertainty threshold is also indicated by the red dashed line in both plots. With the error acceptance range being [-0.2 0.2] mm, it is observed that both models gave sufficiently accurate predictions, especially considering that these predictions were computed online, based on the current knowledge of the models. With a choice of 0.06 for the uncertainty threshold, the proposed selection criterion was effective in the identification of all the holes that showed higher model prediction errors, as all significant prediction errors beyond the required accuracy range were also associated with higher values of the predicted standard deviation. This is consistent with the

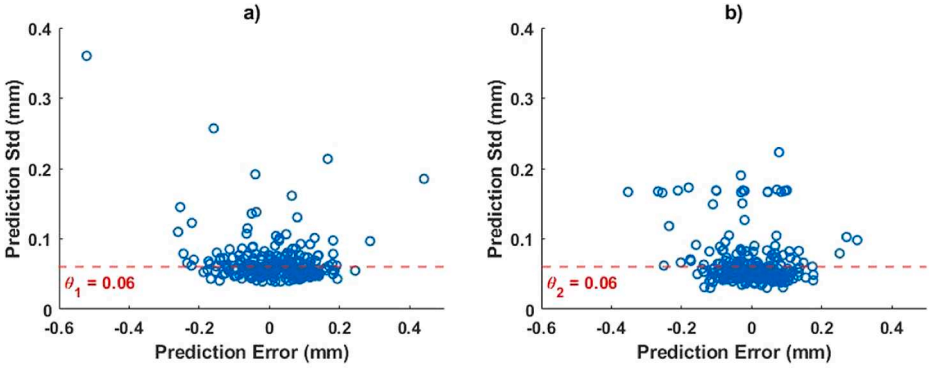

Fig. 10. Scatter plots of the GPR prediction errors against their standard deviations: a) Model 1; b) Model 2.

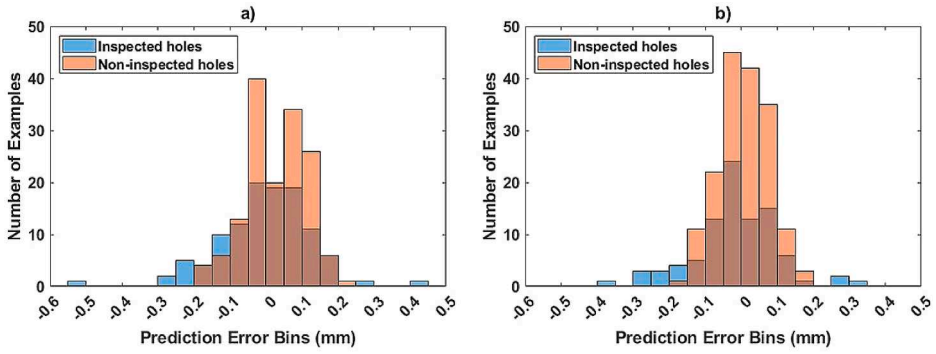

Fig. 11. A histogram representation of the prediction errors of all the holes divided as inspected (blue) and non-inspected (orange): a) Model 1; b) Model 2.

active learning strategy, where the uncertainty threshold is used to request an inspection and expand the current dataset. This inspection request according to the decision made by the learning algorithm avoids making model predictions that would exceed the acceptable error range.

Finally, a histogram representation of the prediction errors obtained by the models for all the machined holes is illustrated in Fig. 11a) Model 1 and b) Model 2. The holes are categorised as inspected holes (in blue), i.e. those which data was included in the training set of the corresponding model, and the non-inspected holes (in orange), i.e. those with lower predicted standard deviations, showing higher model confidence.

The histograms of Fig. 11 emphasise the separation of the holes according to the decision made by the learning algorithm. The prediction error range was considerably reduced from the inspected holes to the non-inspected ones for both models. Most prediction errors for the non-inspected holes were within the [-0.2 0.2] mm interval and [-0.15 0.15] mm for Model 1 and Model 2, respectively. This confirms the ability of the proposed method to successfully identify the holes that didn't require inspection, thus reducing the total number of inspections by 49.3% for Model 1 and 55.9% for Model 2. The prediction accuracies are of comparable magnitude to the Leave-One-Out Cross-Validation (LOO-CV) results of the GPR models obtained in Leco et al. [30] and hence, the active learning represents an efficient modelling strategy.

6. Conclusions

This paper presented an innovative two-step process method to enable right-first-time robotic machining operations. The division of the manufacturing process into two similar steps and the inclusion of an inspection step in between allowed for the prediction and then compensation of the robot-related systematic machining errors. The Gaussian Process Regression (GPR) framework combined with a perturbation-based data generation approach was applied to build and train the models online, without the need for any process interruption. The models predicted the quality of the machined part based on in-process sensory information as opposed to measuring it directly by the post-process inspection step. Moreover, a two-step active learning procedure for making online decisions on the inspection step was implemented and then tested in a robotic countersinking experiment. The proposed method was able to successfully identify the cutting instances that exhibited high confidence in the model predictions and therefore did not require an inspection step. In addition, the instances that contained new information to the current process knowledge were detected using an uncertainty threshold on the GPR model variance prediction. The appropriate information of those instances was added to the model training data in an active learning framework that allowed continual improvement in the prediction accuracies for the subsequent process data. Finally, by correction of the systematic depth errors observed in the first step, the proposed two-step countersinking method was able to achieve final countersink depths within the process tolerance of ±0.2 mm from the desired target, demonstrating the potential of this approach for right-first-time robotic machining.

CRediT authorship contribution statement

Mateo Leco: Conceptualization, Methodology, Software, Validation, Investigation, Data curation, Writing – original draft. **Thomas McLeay:** Conceptualization, Methodology, Supervision. **Visakan Kadirkamanathan:** Investigation, Visualization, Writing – review & editing.

Declaration of Competing Interest

The authors declare that they have no known competing financial interests or personal relationships that could have appeared to influence the work reported in this paper.

Acknowledgments

Funding: This work was supported by the People Programme (Marie Curie Actions) of the European Union's Seventh Framework Programme FP7/2007-2013/ for research, technological development and demonstration [grant number 608022]; and the UK Engineering and Physical Sciences Research Council (EPSRC) [grant reference: EP/P006930/1].

Appendix

A.1 Gaussian Process Regression (GPR)

To take into account the various sources of error affecting the output of the process, a probabilistic learning approach based on Gaussian Process Regression (GPR) [26] has been considered in this work for process modelling.

The GPR is probabilistic approach to regression, which considers inference directly in the function space by generalising the conventional multivariate Gaussian probability to describe a distribution over functions rather than scalars or vectors [26]. In a d-dimensional regression problem, let $\mathscr{D} = \{(\boldsymbol{x}_k, y_k) | k = 1, \ldots, N\}$ denote a training dataset of N instances of pairs of the input vector $\boldsymbol{x}_k \in \mathbb{R}^d$ and the output value $y_k \in \mathbb{R}$. Furthermore, let $f(\boldsymbol{x})$ denote a Gaussian Process (GP) that defines the mapping between the input vector $\boldsymbol{x}$ and the output $y = f(\boldsymbol{x}) + \varepsilon$, where $\varepsilon \sim \mathcal{N}(0, \sigma_n^2)$ is the output measurement noise with variance σ_n^2. In the GPR framework, $f(\boldsymbol{x})$ is assumed to be a random function that can be fully specified by its mean function $m(\boldsymbol{x})$ and the covariance (also called kernel) function $k(\boldsymbol{x}, \boldsymbol{x}')$. Note that the kernel function defines the covariance of the input pairs $\boldsymbol{x}$ and $\boldsymbol{x}'$. In general, a zero mean function is used when the prior information about $f(\boldsymbol{x})$ is scarce, therefore the choice of the kernel function would completely define the GP. A typical kernel choice is the Squared Exponential (SE), also called Gaussian covariance, which assesses the covariance of two input vectors in terms of their Euclidian distance in the d-dimensional space. The kernel function chosen in this work is of the type of the SE covariance performing Automatic Relevance Determination (ARD), which is referred to as the ARD-SE kernel and defined as:

$$k_{ARD}(\boldsymbol{x}, \boldsymbol{x}') = \sigma_f^2 \, exp\left[-\frac{1}{2} \sum_{i=1}^{d} \left(\frac{\| x_i - x_i' \|^2}{l_i^2} \right) \right] \tag{12}$$

where d is the dimension of the input vector $\boldsymbol{x}$, σ_f refers the signal standard deviation and l_i is the individual length-scale hyper-parameter for each input dimension x_i. The ARD is achieved by the fact that each of the input dimensions has an individual l_i. A large value of l_i would lead to a small covariance term for x_i, resulting in an input dimension that has little influence in the inference. The values of the hyper-parameters specified in the covariance function are optimised from the available dataset in the training process using a maximum likelihood estimation approach.

A GPR model makes predictions on new testing points X_* by considering the joint distribution of the observations $\boldsymbol{y}$ (i.e. the training targets) and the new predictions $\boldsymbol{f}_* = f(X_*)$. According to the GP framework, the predictions are computed by conditioning this joint distribution to the training

data (i.e. inputs X and the outputs y), which leads to the following expressions for the conditional mean $\widehat{f}_*$ and covariance $cov(f_*)$ of new testing points X_*:

$$\begin{aligned} \widehat{f}_* &= K(X_*, X)\ \left[K(X,X) + \sigma_n^2 I\right]^{-1}\ y \\ cov(f_*) &= K(X_*, X_*) - K(X_*, X)\ \left[K(X,X) + \sigma_n^2 I\right]^{-1}\ K(X, X_*) \end{aligned} \tag{13}$$

where $K(X_*, X)$, $K(X, X_*)$ and $K(X_*, X_*)$ are the covariance matrices evaluated at all pairs of testing and training points accordingly and with respect to the ARD-SE kernel defined in Eq. (12). Note that Eq. (13) represents the two key predictive expressions of the GPR: the first gives the model predictions on new testing inputs and the second gives the model predictive variance, which is useful additional information on the model reliability.

This work applies GPR models to map the relationship between the sensor signals acquired during the cutting process (input data) and the post-process inspection result (output data). In addition, the ARD-SE kernel defined in Eq. (12) was chosen to select the relevant features during model training. The relevance of each input dimension was assessed based on the value of their length-scale hyper-parameter l_i and the dimensions with major influence in the model's output prediction were selected for further analysis. The reduced input space allowed for efficient model computations and faster prediction times on new unseen data.

References

[1] H.M. Eldessouky, J.M. Flynn, S.T. Newman, On-machine error compensation for right first time manufacture. Procedia Manuf, Elsevier B.V., 2019, pp. 1362–1371, https://doi.org/10.1016/j.promfg.2020.01.152.

[2] K.S. Wang, Towards zero-defect manufacturing (ZDM)-a data mining approach, Adv. Manuf. 1 (2013) 62–74, https://doi.org/10.1007/s40436-013-0010-9.

[3] R. Teti, K. Jemielniak, G. O'Donnell, D. Dornfeld, Advanced monitoring of machining operations, CIRP Ann. - Manuf. Technol. 59 (2010) 717–739, https://doi.org/10.1016/j.cirp.2010.05.010.

[4] R. Teti, Advanced IT Methods of Signal Processing and Decision Making for Zero Defect Manufacturing in Machining, Procedia CIRP (2015) 28, https://doi.org/10.1016/j.procir.2015.04.003.

[5] M.A. Dittrich, B. Schleich, T. Clausmeyer, R. Damgrave, J.A. Erkoyuncu, B. Haefner, J. de Lange, D. Plakhotnik, W. Scheidel, T. Wuest, Shifting value stream patterns along the product lifecycle with digital twins, Procedia CIRP, Elsevier B.V. (2020) 3–11, https://doi.org/10.1016/j.procir.2020.01.049.

[6] C.P. Day, Robotics in Industry—Their Role in Intelligent Manufacturing, Engineering 4 (2018) 440–445, https://doi.org/10.1016/j.eng.2018.07.012.

[7] W. Ji, L. Wang, Industrial robotic machining: a review, Int. J. Adv. Manuf. Technol. 103 (2019) 1239–1255, https://doi.org/10.1007/s00170-019-03403-z.

[8] N. Geier, J.P. Davim, T. Szalay, Advanced cutting tools and technologies for drilling carbon fibre reinforced polymer (CFRP) composites: A review, Compos. Part A Appl. Sci. Manuf. 125 (2019), 105552, https://doi.org/10.1016/j.compositesa.2019.105552.

[9] X. Qiu, P. Li, Q. Niu, A. Chen, P. Ouyang, C. Li, T.J. Ko, Influence of machining parameters and tool structure on cutting force and hole wall damage in drilling CFRP with stepped drills, Int. J. Adv. Manuf. Technol. 97 (2018) 857–865, https://doi.org/10.1007/s00170-018-1981-2.

[10] M. Slamani, S. Gauthier, J.F. Chatelain, Analysis of trajectory deviation during high speed robotic trimming of carbon-fiber reinforced polymers, Robot. Comput. Integr. Manuf. 30 (2014) 546–555, https://doi.org/10.1016/j.rcim.2014.03.007.

[11] M. Slamani, J.F. Chatelain, Assessment of the suitability of industrial robots for the machining of carbon-fiber reinforced polymers (CFRPs), J. Manuf. Process. 37 (2019) 177–195, https://doi.org/10.1016/j.jmapro.2018.11.022.

[12] Y. Chen, J. Gao, H. Deng, D. Zheng, X. Chen, R. Kelly, Spatial statistical analysis and compensation of machining errors for complex surfaces, Precis. Eng. 37 (2013) 203–212, https://doi.org/10.1016/j.precisioneng.2012.08.003.

[13] E. Ferreras-Higuero, E. Leal-Muñoz, J. García de Jalón, E. Chacón, A. Vizán, Robot-process precision modelling for the improvement of productivity in flexible manufacturing cells, Robot. Comput. Integr. Manuf. 65 (2020), 101966, https://doi.org/10.1016/j.rcim.2020.101966.

[14] G. Xiong, Y. Ding, L. Zhu, Stiffness-based pose optimization of an industrial robot for five-axis milling, Robot. Comput. Integr. Manuf. 55 (2019) 19–28, https://doi.org/10.1016/j.rcim.2018.07.001.

[15] T. Cvitanic, V. Nguyen, S.N. Melkote, Pose optimization in robotic machining using static and dynamic stiffness models, Robot. Comput. Integr. Manuf. 66 (2020), 101992, https://doi.org/10.1016/j.rcim.2020.101992.

[16] J. Belchior, M. Guillo, E. Courteille, P. Maurine, L. Leotoing, D. Guines, Off-line compensation of the tool path deviations on robotic machining: Application to incremental sheet forming, Robot. Comput. Integr. Manuf. 29 (2013) 58–69, https://doi.org/10.1016/j.rcim.2012.10.008.

[17] C. Reinl, M. Friedmann, J. Bauer, M. Pischan, E. Abele, O. Von Stryk, Model-based off-line compensation of path deviation for industrial robots in milling applications, in: IEEE/ASME Int. Conf. Adv. Intell. Mechatronics, AIM, 2011, pp. 367–372, https://doi.org/10.1109/AIM.2011.6027113.

[18] Z. Pan, H. Zhang, Robotic machining from programming to process control, Proc. World Congr. Intell. Control Autom. (2008) 499–503, https://doi.org/10.1109/WCICA.2008.4594434.

[19] P.C. Marchal, O. Sörnmo, B. Olofsson, A. Robertsson, J.G. Ortega, R. Johansson, Iterative learning control for machining with industrial robots, IFAC Proc. Vol., IFAC Secretariat (2014) 9327–9333, https://doi.org/10.3182/20140824-6-za-1003.00550.

[20] G. Xiong, Z.L. Li, Y. Ding, L.M. Zhu, A closed-loop error compensation method for robotic flank milling, Robot. Comput. Integr. Manuf. 63 (2020), 101928, https://doi.org/10.1016/j.rcim.2019.101928.

[21] M.F. Zaeh, F. Schnoes, B. Obst, D. Hartmann, Combined offline simulation and online adaptation approach for the accuracy improvement of milling robots, CIRP Ann 69 (2020) 337–340, https://doi.org/10.1016/J.CIRP.2020.04.045.

[22] G. Ge, Z. Du, J. Yang, Rapid prediction and compensation method of cutting force-induced error for thin-walled workpiece, Int. J. Adv. Manuf. Technol. 106 (2020) 5453–5462, https://doi.org/10.1007/S00170-020-05050-1.

[23] W. Zhu, G. Li, H. Dong, Y. Ke, Positioning error compensation on two-dimensional manifold for robotic machining, Robot. Comput. Integr. Manuf. 59 (2019) 394–405, https://doi.org/10.1016/j.rcim.2019.05.013.

[24] C. Wang, Y. Zhao, Y. Chen, M. Tomizuka, Nonparametric statistical learning control of robot manipulators for trajectory or contour tracking, Robot. Comput. Integr. Manuf. 35 (2015) 96–103, https://doi.org/10.1016/j.rcim.2015.03.002.

[25] V. Nguyen, T. Cvitanic, S. Melkote, Data-Driven Modeling of the Modal Properties of a Six-Degrees-of-Freedom Industrial Robot and Its Application to Robotic Milling, J. Manuf. Sci. Eng. (2019) 141, https://doi.org/10.1115/1.4045175.

[26] C.E. Rasmussen, Gaussian Processes in machine learning, Lect. Notes Comput. Sci. (Including Subser. Lect. Notes Artif. Intell. Lect. Notes Bioinformatics). 3176 (2004) 63–71, https://doi.org/10.1007/978-3-540-28650-9_4.

[27] Y. Chen, J. Chen, G. Xu, A data-driven model for thermal error prediction considering thermoelasticity with gated recurrent unit attention, Meas. J. Int. Meas. Confed. 184 (2021).

[28] W. Chengyang, X. Sitong, X. Wansheng, Spindle thermal error prediction approach based on thermal infrared images: A deep learning method, J. Manuf. Syst. 59 (2021) 67–80, https://doi.org/10.1016/J.JMSY.2021.01.013.

[29] M. Papananias, T.E. McLeay, O. Obajemu, M. Mahfouf, V. Kadirkamanathan, Inspection by exception: A new machine learning-based approach for multistage manufacturing, Appl. Soft Comput. 97 (2020), 106787, https://doi.org/10.1016/j.asoc.2020.106787.

[30] M. Leco, V. Kadirkamanathan, A perturbation signal based data-driven Gaussian process regression model for in-process part quality prediction in robotic countersinking operations, Robot. Comput. Integr. Manuf. 71 (2021), 102105, https://doi.org/10.1016/j.rcim.2020.102105.

[31] Y. Fu, X. Zhu, B. Li, A survey on instance selection for active learning, Knowl. Inf. Syst. 35 (2013) 249–283, https://doi.org/10.1007/s10115-012-0507-8.

[32] S.J. Huang, R. Jin, Z.H. Zhou, Active Learning by Querying Informative and Representative Examples, IEEE Trans. Pattern Anal. Mach. Intell. 36 (2014) 1936–1949, https://doi.org/10.1109/TPAMI.2014.2307881.

[33] X. Zhu, P. Zhang, X. Lin, Y. Shi, Active Learning from Data Streams, in: Seventh IEEE Int. Conf. Data Min. (ICDM 2007), IEEE, 2007, pp. 757–762, https://doi.org/10.1109/ICDM.2007.101.

[34] G. Martínez-Arellano, S. Ratchev, Towards an active learning approach to tool condition monitoring with bayesian deep learning, in: Proc. - Eur. Counc. Model. Simulation, ECMS, European Council for Modelling and Simulation, 2019, pp. 223–229, https://doi.org/10.7148/2019-0223.

[35] B. Botcha, A.S. Iquebal, S.T.S. Bukkapatnam, Efficient manufacturing processes and performance qualification via active learning: Application to a cylindrical plunge grinding platform, Procedia Manuf 53 (2021) 716–725, https://doi.org/10.1016/J.PROMFG.2021.06.070.